JACS
JOURNAL OF THE AMERICAN CHEMICAL SOCIETY
Article
pubs.acs.org/JACS

Reactivity-Based Detection of Copper(II) Ion in Water: Oxidative Cyclization of Azoaromatics as Fluorescence Turn-On Signaling Mechanism

Junyong Jo, Ho Yong Lee, Wenjun Liu, András Olasz, Chun-Hsing Chen, and Dongwhan Lee*

Department of Chemistry, Indiana University, 800 East Kirkwood Avenue, Bloomington, Indiana 47405, United States

Supporting Information

ABSTRACT: An oxidative cyclization reaction transforms nonemissive azoanilines into highly fluorescent benzotriazoles. We have found that introduction of multiple electron-donating amino groups onto a simple *o*-(phenylazo)aniline platform dramatically accelerates its conversion to the emissive polycyclic product. Notably, this chemistry can be effected by μM-level concentrations of copper(II) ion in water (pH = 6−8) at room temperature to elicit >80-fold enhancement in the green emission at λ_{em} = 530 nm. Comparative kinetic and electrochemical studies on a series of structural analogues have established that the accelerated reaction rates correlate directly with a systematic cathodic shift in the oxidation onset potential of the azo precursors. In addition, single-crystal X-ray crystallographic analysis on the most reactive derivative revealed the presence of a five-membered ring intramolecular hydrogen-bonding network. An enhanced contribution of the quinoid-type resonance in such conformation apparently facilitates the mechanistically required proton transfer step, which, in conjunction with electron transfer at lower oxidation potential, contributes to a rapid cyclization reaction triggered by copper(II) ion in water.

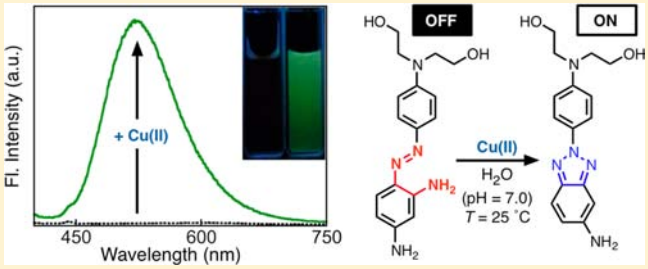

INTRODUCTION

Small molecule fluorophores that target heavy metal ions have broader impacts on multiple disciplines including biological imaging, medical diagnostics, industrial process control, and environmental monitoring.[1] As enzyme cofactors and signal messengers, copper plays many important roles in living system,[2] but a high level of unbound copper ions has deleterious effects, including oxidative damage or misfolding of proteins responsible for many neurodegenerative diseases.[3]

For open-shell metal ions, such as copper(II), multiple nonemissive de-excitation pathways involving electron transfer or excited-state energy transfer are typically available to quench fluorescence.[4] As such, existing fluorescent chelates that respond to copper(II) exploit dual emission from internal charge transfer (ICT) and shifts in wavelength,[5] rather than a straightforward enhancement in fluorescence intensity upon metal binding.[6]

An alternative approach is reactivity-based detection, which utilizes irreversible chemical reactions to transform nonemissive precursors to fluorescent products and tracks time-dependent cumulative effects of metal exposure.[7] For example, ring opening or hydrolysis of certain designer molecules is accelerated by copper(II) ion functioning as a Lewis acid.[8]

Within this context, we envisioned that an enhancement in fluorescence signal that is induced by the *redox activity* of copper(II) ion could be an appealing design strategy, which should not suffer from background signals from potentially competing Lewis acids in the hydrolysis-based detection schemes.[8] In addition to addressing the requirements for turn-on signaling that is tightly coupled to the selective recognition and/or triggering event, copper(II)-responsive probes need to operate in water under ambient conditions for practical applications in detection and imaging. Macromolecular systems built with copper(II)-dependent DNAzymes meet such requirements.[9] Small molecule turn-on fluorescence probes that are compatible with genuine aqueous environments are exceedingly rare,[8j,k] which further highlights ongoing challenges in this research area.

During our search for a promising model system in which copper(II) functions as an oxidant to convert nonemissive reactant to emissive product, we came across the oxidative cyclization of *o*-(phenylazo)aniline (**1**) to benzotriazole (**2**) shown in Scheme 1.[10] Despite its conceptual appeal of converting a nonemissive azo dye **1** to a highly fluorescent product **2**, this chemistry typically requires an extended reaction time in basic organic solvents at elevated temperatures,[10−12] which significantly diminishes its practical utility as

Scheme 1. Synthetic Routes to Benzotriazoles

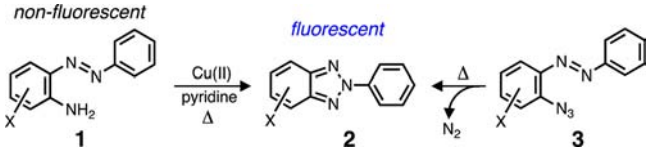

Received: July 25, 2012
Published: August 30, 2012

a detection method for copper(II) ion under ambient and biologically relevant conditions.

Taking inspirations from this straightforward functional group transformation that profoundly impacts molecular photophysics, we have investigated a series of structural analogues **4**–**8** shown in Scheme 2. A strategic placement of

Scheme 2. Chemical Structures of Functionalized Azoanilines

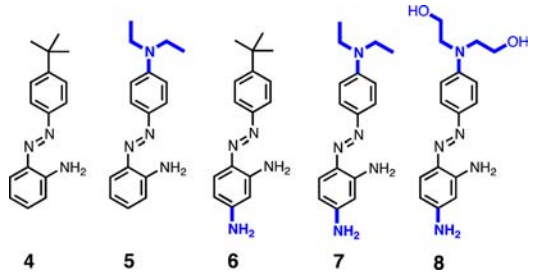

electron-donating and water-solubilizing amine groups onto the simple *o*-(phenylazo)aniline platform dramatically accelerated the oxidative cyclization reaction in water, as demonstrated by the turn-on fluorescence response of **8** toward ppm-level of copper(II) ions in water at neutral pH. A coherent structure–reactivity relationship that emerges from a combination of kinetic, electrochemical, X-ray crystallographic, and computational studies constitutes the main topic of this paper, the details of which are provided in the following sections.

BACKGROUND: FROM AZO TO TRIAZOLE

The thermal decomposition of *o*-azidoazobenzene **3** is one of the oldest known synthetic routes to benzotriazole **2** and its analogues (Scheme 1),[13,14] which was reported as early as in 1887.[15] More conveniently, **2** is prepared by the oxidation of azoaniline **1** (Scheme 1), a synthetically more accessible precursor that can be subjected to large-scale laboratory manipulations. As shown in Scheme 3, oxidative cyclization

Scheme 3. Oxidative Cyclization of Azoaniline[a]

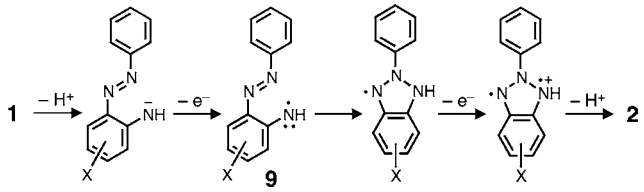

[a]For clarity, coordination of metal ions to the amino/azo N-donor is not shown. Alternative sequences of electron- and proton-transfer (ET and PT, respectively) steps could also be considered that avoid the development of highly charged intermediates in the net removal of $2H^+/2e^-$ from **1** to form **2**.

of **1** proceeds via a net loss of two protons and two electrons, and is driven by the stability of the newly formed heteroaromatic triazole ring of **2**. With Pb(IV) or Cu(II) as an oxidant, the **1** → **2** conversion is postulated to involve the areneamino radical intermediate **9** (Scheme 3),[11,16,17] which undergoes intramolecular N–N coupling rather than intermolecular dimerization. Coordination of metal ions to the *N*-donor group assists the consecutive deprotonation/oxidation steps as the entry point to this chemistry.[18]

The mechanistic framework outlined in Scheme 3 served as a good starting point for our structure design to enhance the chemical reactivity of the parent system **1**. Specifically, we wished to introduce chemical functionalities that can promote the oxidation, deprotonation, or a combination of both.

RESULTS AND DISCUSSION

Design and Synthesis. A series of *o*-(phenylazo)aniline derivatives **4**–**8** were designed (Scheme 2) and prepared in a straightforward manner (Scheme 4). Along the series

Scheme 4. Synthetic Routes to Functionalized Azoanilines and Benzotriazoles[a]

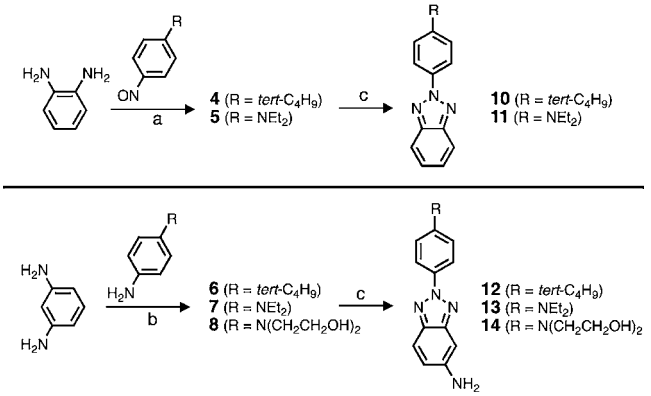

[a](a) KOH or NaOH, toluene, Δ. (b) (i) aq HCl/$NaNO_2$, MeOH; (ii) aq NaOH, MeOH, 0 °C. (c) $Cu(OAc)_2$, MeCN or THF, pyridine, Δ.

5 → **6** → **7**, an increasing number of electron-donating amine groups were installed either in the upper (= phenyl) or lower (= aniline) ring of the *o*-(phenylazo)aniline platform of the benchmark system **4**. For the compound **8**, two hydroxyl groups were introduced as part of *N*-alkyl tethers to enhance the water solubility of **7**, the most electron-rich system.

As summarized in Scheme 4, simple condensation reactions between *para*-substituted nitrosobenzenes and *o*-phenylenediamine produced **4** and **5**. Compounds **6**–**8** were prepared in high yields (88–95%) from *m*-phenylenediamine and the corresponding diazonium salts, generated *in situ* under standard azo coupling conditions. Preparative-scale transformation of **4**–**8** to the corresponding benzotriazole products **10**–**14** (Scheme 4) was achieved by using copper(II) as oxidant and pyridine as base.

Photophysical Properties. With a series of functionalized benzotriazoles **10**–**13** (Scheme 4) in hand, we investigated their photophysical properties. Unlike their precursors **4**–**7**, which are nonemissive as typical azo dyes, photoexcited **10**–**13** are highly fluorescent (Figure 1). Notably, the fluorescence quantum yield (= Φ_F) of **10** is essentially 100% (in MeCN) when excited at λ = 320 nm. Substitution on the benzotriazole core and/or the *N*-aryl ring did not significantly compromise the emission efficiency, with Φ_F = 26–42% determined for **11**–**13** in MeCN (Table 1).

The fluorescence spectra of **10**–**13** in MeCN (Figure 1a) also revealed systematic red-shifts ($\Delta\lambda$ = 70 nm) in the emission energy along the series **10** → **12** → **13** → **11**. This empirical trend apparently reflects the charge-separated nature of the excited states,[19] which involve electron-deficient benzotrizole core and electron-rich *N*-aryl substituent part of the molecule. As can be anticipated from the chemical

dx.doi.org/10.1021/ja307316s | J. Am. Chem. Soc. 2012, 134, 16000–16007

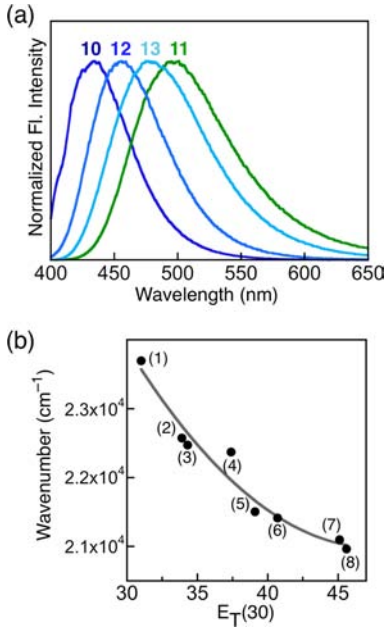

Figure 1. (a) Normalized emission spectra of **10**–**13** in MeCN. (b) Polarity-dependent shifts in the emission maximum of **13** plotted as wavenumber (cm^{-1}) vs $E_T(30)$ for various solvents including hexane (1), benzene (2), toluene (3), THF (4), $CHCl_3$ (5), CH_2Cl_2 (6), MeCN (7), and DMSO (8). T = 298 K.

Table 1. Photophysical Properties of Functionalized Benzotriazoles

compound	$\lambda_{max,abs}$ (nm)	$\lambda_{max,em}$ (nm)	Φ_F (%)[a]
10	310	430	100
11	370	500	42
12	360	455	26
13	380	480	39

[a]In MeCN at T = 298 K.

structures (Scheme 4), such charge-transfer (CT)-type emission should be most pronounced for **11**. Structurally related **13** also displays strong solvent-dependent fluorescence spectra (Figure S1) with an excellent linear correlation between the emission energy and $E_T(30)$ values (Figure 1b).[20] On the other hand, the emission from the reference system **10** remains largely insensitive to solvent polarity (Figure S2). With appropriate functionalization, the charge-separated excited-states of *N*-aryl benzotriazoles should thus produce longer-wavelength emission in polar aqueous environments (*vide infra*), with large Stokes shifts (Table 1; Figure S3) to minimize fluorescence reabsorption or self-quenching.

Fluorescence Kinetic Studies: Structure–Reactivity Relationships. In order to explore the functional role of the electron-donating aryl substituents in the reaction mechanism shown in Scheme 3, we decided to carry out comparative kinetic studies on the oxidative cyclization of **4**–**7**. As shown in Figure 2a, the reaction between the nonemissive azoaniline **7** and $Cu(OAc)_2$ in MeCN proceeds at room temperature with no added base to furnish a highly fluorescent product, the emission spectrum of which is essentially superimposable with that of the benzotriazole **13** (Figure 2b), prepared and characterized independently (Figure 2c).

Under pseudo-first-order reaction conditions (>300 equiv of $[Cu^{2+}]$ with respect to the azo precursor **7**), the formation of

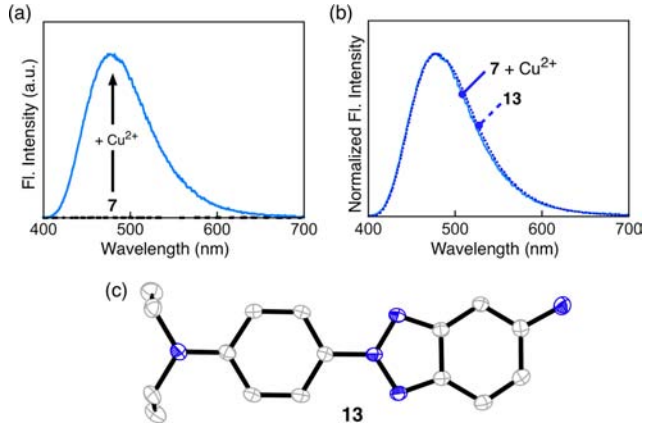

Figure 2. (a) Emission spectra (λ_{exc} = 380 nm) of **7** in MeCN mixed with 3% (v/v) H_2O, prior to (black dotted line) and after (blue solid line) addition of $Cu(OAc)_2$ (100 equiv) at T = 298 K. (b) Normalized fluorescence spectra of the (i) **7** + $Cu(OAc)_2$ reaction mixture (blue solid line) and (ii) **13** (blue dotted line). (c) X-ray structure of **13** as ORTEP diagrams with thermal ellipsoids at 50% probability.

the product **13** was monitored by time-dependent enhancement in the fluorescence intensity at λ_{em} = 480 nm (= $\Delta I_{480\ nm}$; λ_{exc} = 380 nm) in MeCN with 3% (v/v) H_2O at T = 298 K. The exponential increase in $\Delta I_{480\ nm}$ as a function of time was fitted using eq 1 to determine the pseudo-first-order rate constant k' (Figures 3a and S4):

$$\frac{\Delta I}{I} = 1 - e^{-k't} \quad (1)$$

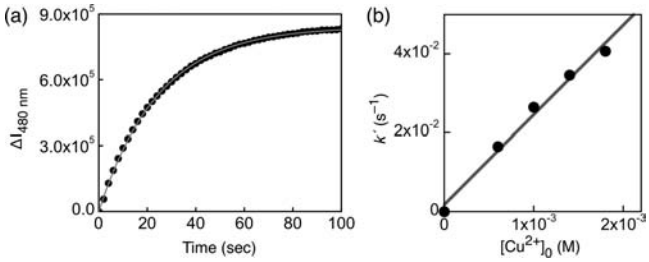

Figure 3. (a) Time-dependent changes in the fluorescence intensity at λ = 480 nm (λ_{exc} = 380 nm) observed for the reaction between **7** (2.0 μM) and Cu^{2+} (1.8 mM) in MeCN mixed with 3% (v/v) H_2O at T = 298 K. The gray curve overlaid on the experimental data points is a theoretical fit generated using $k' = 4.07 \times 10^{-2}$ s^{-1} and eq 1. (b) A plot of k' (=$k[Cu^{2+}]_0$) vs $[Cu^{2+}]_0$ to determine the second-order rate constant k = 23 ± 1 M^{-1} s^{-1}.

A linear dependence of k' (= $k[Cu^{2+}]_o$; eq 1) on $[Cu^{2+}]_o$ (Figure 3b) established that the reaction proceeds via bimolecular rate-limiting step with first-order in both copper(II) ion and azo dye, and the second-order rate constant of k = 23 ± 1 M^{-1} s^{-1}. Under similar conditions, the compounds **5** and **6** also react with copper(II) in second-order fashion to furnish **11** and **12**, respectively (Figures S5 and S6), but their formation kinetics are significantly slower. Specifically, the second-order rate constants of k = 0.54 ± 0.05 M^{-1} s^{-1} determined for the conversion of **5** → **11** and 0.73 ± 0.06 M^{-1} s^{-1} for the conversion of **6** → **12** are ca. 30–40-times slower than that of **7** at T = 298 K. The simple azoaniline reference system **4** does not even react with copper(II) at room temperature. Our kinetic studies have thus established the

dx.doi.org/10.1021/ja307316s | J. Am. Chem. Soc. 2012, 134, 16000–16007

reactivity order of 7 > 6 ∼ 5 ≫ 4, which correlates directly with the number of amine groups that are introduced to the common *o*-(phenylazo)aniline platform (Scheme 2).

Electrochemical Studies: Structure−Property Relationships. As depicted in Scheme 3, oxidative cyclization of azoanilines is postulated to proceed via consecutive PT−ET steps. Our kinetic studies described in the previous section have established that electron-rich azoanilines display faster response to copper(II) ions in the bimolecular reaction. In order to obtain a quantitative understanding of the relationship between the thermodynamics of oxidation and the kinetics of ring closure, we carried out electrochemical studies on **4**−**7**.

Under typical conditions used for cyclic voltammetry (CV), the unsubstituted azoaniline **4** showed an irreversible oxidation wave with the onset potential of $E_{ox/onset}$ = 0.55 V (Figure 4).[21]

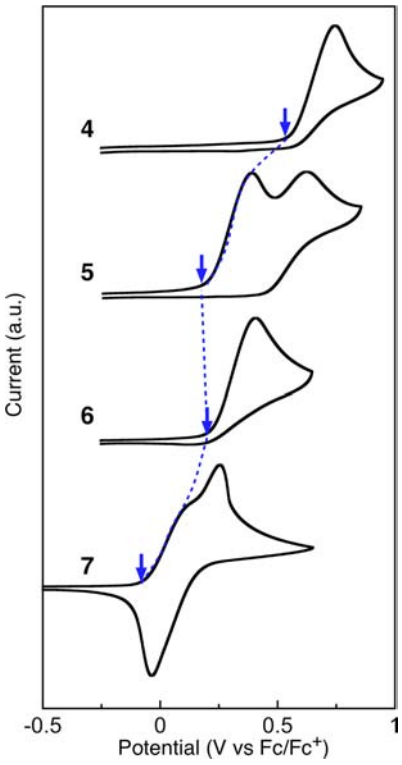

Figure 4. CVs of **4**−**7** (sample concentration = 3.5 mM) in CH_2Cl_2 with $^nBu_4NPF_6$ (0.1 M) as supporting electrolyte (scan rate = 100 mV/s; T = 298 K). For each CV, the oxidation onset potential is indicated by a vertical arrow.

Introduction of additional amine group, either in the upper ring of **5** ($E_{ox/onset}$ = 0.20 V) or in the lower ring of **6** ($E_{ox/onset}$ = 0.21 V), resulted in significant cathodic shifts of the oxidation potential (Figures 4). With both the upper and lower rings functionalized with amine groups, compound **7** has the most cathodically shifted $E_{ox/onset}$ value of −0.06 V. A systematic cathodic shift in the oxidation onset potentials of **7** > **6** ∼ **5** > **4** (Figure 4; Table 2) observed here correlates nicely with the second-order rate constants for the oxidative cyclization of **7** > **6** ∼ **5** ≫ **4** (Figures 3 and S4−S6; Table 2).

The reaction mechanism postulated in Scheme 3 most likely requires coordination of the copper(II) ion to the amine/amide nitrogen atom to facilitate both PT and ET, with the possibility of azo nitrogen atom functioning as an additional ligand to assist metal binding.[22] Our electrochemical studies now suggest that the rate-limiting step in this cyclization reaction involves

Table 2. Oxidation Potential and Rate Constant of Oxidative Cyclization of Azoanilines (T = 298 K)

compound	$E_{ox/onset}$ (V)[a]	k_2 (M^{-1} s^{-1})
4	0.55	−[b]
5	0.20	0.54 ± 0.05
6	0.21	0.73 ± 0.06
7	−0.06	23 ± 1

[a]Onset oxidation potential referenced to Fc/Fc^+. [b]No reaction.

ET, rather than PT. This interpretation is based on the assumption that the trend observed for electrochemically determined $E_{ox/onset}$ values (Figure 4) reflects the facility with which inner-sphere ET occurs from the amine/amide group to the copper(II) ion functioning as a chemical oxidant.

X-ray Crystallographic Studies: Functional Role of π-Conjugation and Hydrogen Bonds. An increasing number of electron-donating groups enhance the chemical reactivity of azoanilines toward oxidative cyclization. While this intuitive structure−reactivity relationship was validated and reinforced by a combination of kinetic and electrochemical studies described in previous sections, we wondered whether such redox argument could solely account for the remarkable reactivity of **7** compared with its structural analogues **4**−**6**. X-ray crystallographic studies on **7** provided significant insights into this question.

A single crystal of **7** was obtained by vapor diffusion of pentane into a methanol solution and subjected to crystallographic structure analysis. Intriguingly, **7** exists as two rotational isomers **7A** and **7B** (Figure 5a) in the solid-state, which are

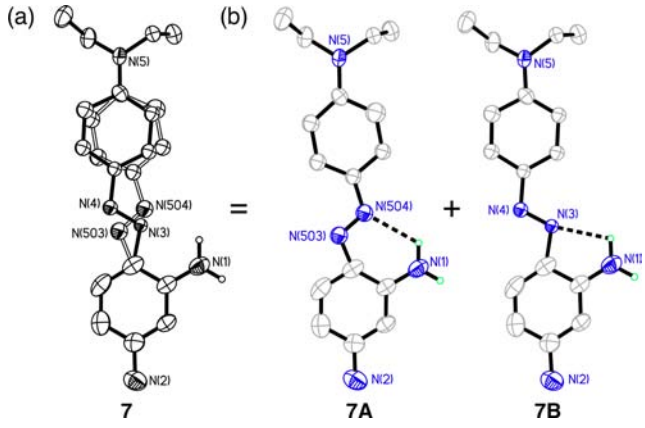

Figure 5. (a) X-ray structure of **7** as ORTEP diagrams with 50% thermal ellipsoids. The two conformations **7A** (site occupancy = 32%) and **7B** (site occupancy = 68%) constituting the disorder are shown in (b).

related by ca. 180° rotation around the C−N bond. In the rotamer **7A** (Figure 5b), the Nα atom of the azo group is engaged in a typical six-membered intramolecular hydrogen bonding with the *ortho*-NH_2 group (N···N = 2.884 Å).[23,24] The major (68%) component of the solid-state structure of **7**, however, is represented by the other rotamer **7B** (Figure 5b), which has a rather unusual five-membered intramolecular hydrogen bonding between the Nβ atom of the azo group and the amine N−H group (N···N = 2.603 Å).[25] An equilibrium between six- and five-membered "chelate" rings through N−H···N hydrogen bond was suggested by UV−vis spectroscopic studies on a structurally related molecule.[26,27] Prior to our

dx.doi.org/10.1021/ja307316s | J. Am. Chem. Soc. 2012, 134, 16000−16007

work, however, no structural evidence has been reported to support this notion.

The solid-state structure of the azo compound **7** thus reflects a conformational equilibrium between **7A** and **7B** with contributions from the hydrazone resonance structure (Scheme 5). In order to confirm that such conformational bistability has

Scheme 5. Conformational Bistability of 7A and 7B through (i) Formation of the Six- vs Five-Membered Hydrogen Bond and (ii) Contribution of the Zwitterionic Resonance Structure

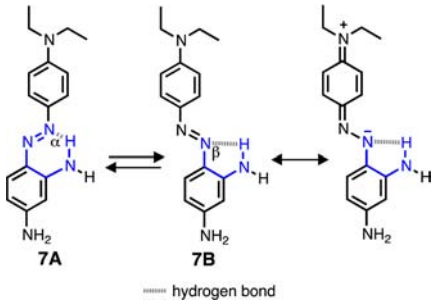

its origin in the intrinsic thermodynamic properties of the molecule, we carried out geometry optimization at the MP2 level of theory (with a triple-ζ basis set) on the simplified models **7A′** and **7B′**, in which the *p*-diethylamino group of the parent system has been replaced with a simpler *p*-dimethylamino moiety.

As shown in Figure 6, the energy-minimized structures **7A′** and **7B′** are essentially superimposable onto the crystallo-

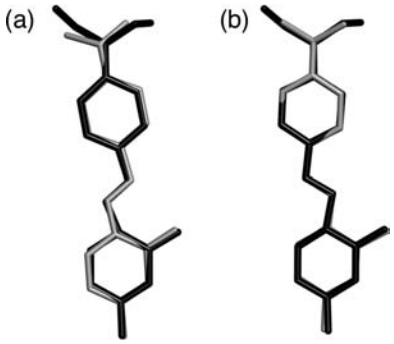

Figure 6. An overlay of the X-ray structures of (a) **7A** and (b) **7B** (in black) with the corresponding MP2/TZVP models **7A′** and **7B′** (in gray), respectively.

graphically determined atomic coordinates of **7A** and **7B**, respectively. More importantly, the energy difference between **7A′** and **7B′** is as small as 0.6 kcal mol^{-1}.[28]

The coexistence of the two essentially isoenergetic rotamers of **7** presumably reflects a fine balance between (i) steric preference for the unstrained six-membered hydrogen bond of **7A** with the N−H···Nα contact and (ii) electronic preference for the five-membered hydrogen bonding of **7B** with the N−H···Nβ contact to stabilize the zwitterionic resonance structure. We postulate that this five-membered hydrogen bond should allow the azo Nβ position to interact directly with the *ortho*-amino group and activate its N−H bond for deprotonation and subsequent oxidation (Scheme 3). In addition to the electronic factors responsible for the lowered oxidation potential, a synergistic interplay between the π-conjugation and the intramolecular hydrogen bond might thus contribute to the remarkable reactivity of **7** relative to its analogues **4**−**6**.

Fluorescence Turn-On Detection of Copper(II) Ion in Water. With a better understanding of the structure−property−reactivity relationships obtained for the azo precursors **4**−**7** and their cyclization products **10**−**13**, we investigated the scope of this chemistry in physiologically relevant environment. Using **7** as template, **8** was designed to enhance the water solubility of the parent system but without compromising its high reactivity. With the key structural features of amine-functionalized azoaniline platform retained, installation of hydroxyl groups as part of the *N*-alkyl tethers rendered **8** soluble up to 30 μM in buffered (pH = 7) water (Figure S7). A linear relationship between the concentration and the absorbance indicated no intermolecular association under this condition.

Upon exposure to copper(II) in water (pH = 7.0; HEPES, 50 mM), the strong absorption of **8** at $\lambda_{max,abs}$ = 475 nm, which is characteristic of its azo chromophore, rapidly lost its intensity. This process is accompanied by concomitant build-up of a new blue-shifted feature at $\lambda_{max,abs}$ = 375 nm from the cyclized product **14** (Figure 7a). This metal-induced chemical transformation could be monitored in a straightforward manner by a large (>80-fold) enhancement in the fluorescence intensity at $\lambda_{max,em}$ = 530 nm, which is discernible even by naked eyes (Figure 7b). No interference, such as paramagnetic quenching,

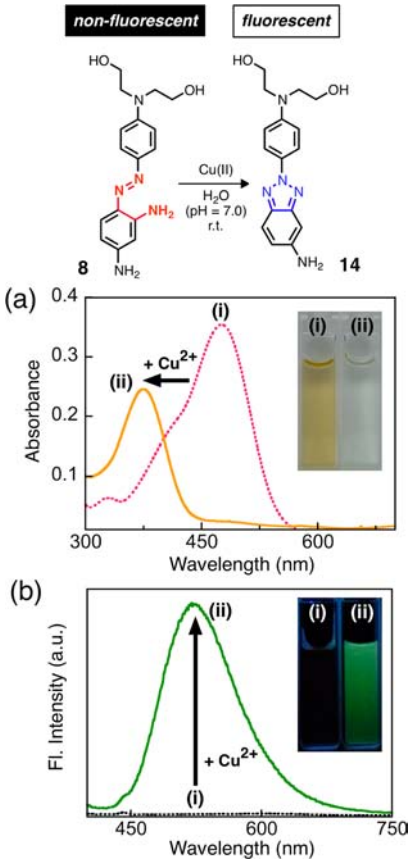

Figure 7. Oxidative cyclization of **8** (10 μM) to **14**, triggered by copper(II) ions (100 equiv) in water (pH = 7.0; HEPES, 50 mM) and monitored by (a) UV−vis and (b) fluorescence spectroscopy after 10 min. Digital images in the insets were obtained (with ambient light for (a), and a hand-held UV lamp (λ_{exc} = 365 nm) for (b)) for the samples prepared using the same experimental conditions.

dx.doi.org/10.1021/ja307316s | J. Am. Chem. Soc. 2012, 134, 16000−16007

by free copper(II) ion was observed, presumably due to the weak metal-binding affinity of the triazole or *N*,*N*-diethanolamine groups in aqueous environment.

The practical utility of **8** was demonstrated further by the (i) consistent turn-on fluorescence response to copper(II) in water in the physiologically/environmentally relevant pH window of 6−8 (Figure 8a) but no fluorescence signaling at pH < 5.5,[29] (ii) high sensitivity to the ppm-level concentrations of copper(II) (Figure 8b), and (iii) high selectivity toward copper(II) in the presence of various metal ions (Figure 8c,d).[30] A plot of $\Delta I_{530\ nm}$ vs copper concentration in Figure 8b shows an excellent linear relationship down to the value of $[Cu^{2+}]$ = 10 μM, which is comparable to the U.S. Environmental Protection Agency (EPA) guideline of 1.3 ppm (= 21 μM) copper(II) ion in drinking water.[31]

SUMMARY AND OUTLOOK

An efficient chemical transformation of nonemissive azoanilines to highly fluorescent benzotriazoles was exploited for the turn-on fluorescence detection of copper(II) ion in aqueous solutions at room temperature. The most optimized system responds selectively to ppm-level copper(II) at pH = 6−8 but remains latent in acidic (pH < 5.5) environment. Comparative kinetic and electrochemical studies on a series of model compounds have established that the oxidation potential of the precursor correlates directly with the rate of cyclization, which is accelerated by an increasing number of amine substituents installed on the common azoaniline platform. X-ray crystallographic and computational studies provided significant insights into the potential functional role of intramolecular hydrogen bonds and π-conjugated electron-donor groups in this reactivity-based metal detection scheme.

In addition to the turn-on fluorescence signaling with a large Stokes shift, the energy of the CT-type emission of the cyclization product is strongly dependent on the solvent polarity. Such features should be advantageous in tracking copper(II) ions in biological samples, for which information on the local dielectric could also be obtained in a simultaneous fashion by polarity-sensitive shifts in the emission wavelength. Efforts are currently underway in our laboratory to improve the photophysical properties of this first-generation proof-of-principle system for such advanced applications.

EXPERIMENTAL SECTION

General Considerations. All reagents were obtained from commercial suppliers and used as received unless otherwise noted. The solvents acetonitrile, hexane, tetrahydrofuran, and dichloromethane were saturated with nitrogen and purified by passage through activated Al_2O_3 columns under nitrogen (Innovative Technology SPS 400). All air-sensitive manipulations were carried out under nitrogen atmosphere by standard Schlenk-line techniques. The compounds *N*,*N*-bis(2-hydroxyethyl)-4-amino-aniline[32] and 4-*tert*-butyl nitrosobenzene[33] were prepared according to literature procedures.

Physical Measurements. ^{1}H NMR and ^{13}C NMR spectra were recorded on a 400 MHz Varian Inova NMR spectrometer. Chemical shifts were reported versus tetramethylsilane and referenced to the residual solvent peaks. High-resolution chemical ionization (CI) (using CH_4 as CI reagent) and electrospray ionization (ESI) mass spectra were obtained on a Thermo Electron Corporation MAT 95XP-Trap. High-resolution GC-MS (CI, using CH_4 as CI reagent) was obtained on a Thermo Electron Corporation MAT 95XP-Trap. FT-IR spectra were recorded on a Nicolet 510P FT-IR spectrometer with EZ OMNIC ESP software. UV−vis spectra were recorded on an Agilent 8453 UV−vis spectrophotometer with ChemStation. Fluorescence spectra were recorded on a Photon Technology International QM-4-CW spectrofluorometer with FeliX32 software.

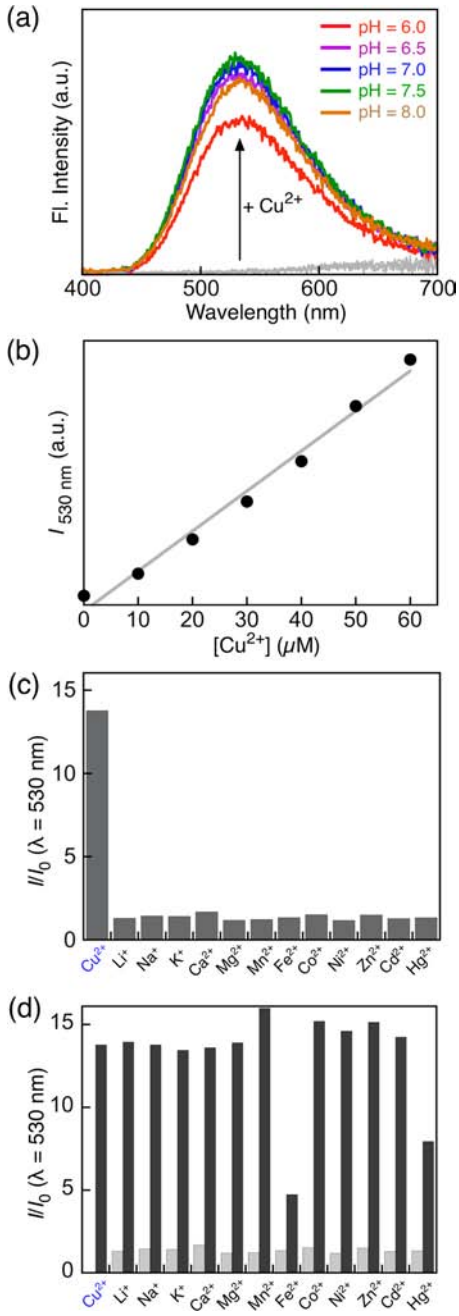

Figure 8. (a) Changes in the emission spectra of **8** (10 μM) after exposure to copper(II) (1.0 mM) in water at pH = 6.0−8.0 (MES buffer for pH = 6.0−6.5; HEPES buffer for pH = 7.0−8.0; 50 mM). (b) A plot of fluorescence intensity at λ = 530 nm of **8** (10 μM) vs concentration of copper(II) in water at pH = 7.0 (HEPES, 50 mM). (c) Fluorescence response of **8** (10 μM) toward metal ions in water at pH = 7.0 (HEPES, 50 mM). The signal intensity at λ = 530 nm (= I) is normalized with that of the probe-only sample (= I_0). The bars represent I/I_0 of **8** in the presence of various metal ions (100 equiv) screened. (d) Selectivity of **8** (10 μM) for copper(II) in the presence of other metal ions. The light-gray bars represent the I/I_0 value in the presence of various metal ions (100 equiv) screened. The black bars indicate the change in the emission intensity upon subsequent addition of copper(II) (100 equiv) to the solution containing **8** and the metal ion of interest. For all measurements, λ_{exc} = 380 nm; T = 298 K.

dx.doi.org/10.1021/ja307316s | J. Am. Chem. Soc. 2012, 134, 16000−16007

Fluorescence Quantum Yield Measurements. Quantum yields were determined by standard methods,[34] using coumarin 30 (Φ_F = 0.67 in MeCN solution; λ_{exc} = 380 nm) or *trans,trans*-1,4-diphenyl-1,3-butadiene (Φ_F = 0.42 in hexane solution; λ_{exc} = 320 nm) as a standard. The sample absorbance was maintained < 0.1 to minimize internal absorption. Corrections were made to account for the differences in solvent refractive indexes.

Reactivity Studies. A stock solution of **8** (5.0 mM) in DMSO was diluted with buffered H_2O (pH = 7.0; HEPES, 50 mM) to prepare sample solutions (10 μM; 0.2% DMSO (v/v) in H_2O). Solution samples (40 mM) of metal ions Cu^{2+}, Li^+, Na^+, K^+, Ca^{2+}, Mg^{2+}, Mn^{2+}, Fe^{2+}, Co^{2+}, Ni^{2+}, Zn^{2+}, Cd^{2+}, and Hg^{2+} were prepared by dissolving the corresponding salt in water. In order to minimize dilution effects, a 75 μL aliquot of each metal ion stock solution (= 100 equiv with respect to **8**) was delivered using a microsyringe into a 3.0 mL sample solution of **8** placed in a thermostatted Peltier cuvette holder.

Kinetic Studies. Comparative kinetic studies on **4**−**7** were carried out in MeCN by delivering an aqueous solution sample (30−90 μL) of $Cu(OAc)_2$ into a MeCN solution sample (3.0 mL) of each reactant placed in a thermostatted (T = 298 K) Peltier cuvette holder. The total amount of water in this mixed solvent system was maintained constant (90 μL; 3% H_2O (v/v) in MeCN) by adding an appropriate (0−60 μL) amount of H_2O to the solution prior to the injection of the copper(II) reagent. With constant stirring, the time-dependent changes in the fluorescence intensity were monitored at the maximum emission wavelength of each compound: λ = 450 nm for **4** (λ_{exc} = 350 nm) and **6** (λ_{exc} = 360 nm); λ = 480 nm for **5** (λ_{exc} = 370 nm) and **7** (λ_{exc} = 380 nm). The ΔI vs t kinetic traces were fitted by a nonlinear regression method (OriginPro 8.6) using eq 1, in which the parameters k' (= $k[Cu^{2+}]_0$) and I (= intensity at $t \rightarrow \infty$) were allowed to vary.

Electrochemistry. Electrochemical studies were carried out under ambient atmosphere with an Autolab Model PGSTA30 potentiostat (Eco Chemie). A three-electrode configuration consisting of a working electrode (glassy carbon electrode), a $Ag/AgNO_3$ (0.01 M in MeCN with 0.1 M $^nBu_4NPF_6$) reference electrode, and a platinum coil counter electrode was used. All electrochemical potentials are reported to the Cp_2Fe/Cp_2Fe^+ redox couple.

4-[((*N*,*N*-Bis(2-hydroxyethyl)-4-amino)phenyl)azo]-1,3-benzenediamine (8). To a stirred MeOH solution (10 mL) of *N*,*N*-bis(2-hydroxyethyl)-4-amino-aniline (1.73 g, 7.67 mmol) was added slowly conc. HCl (2.5 mL). The reaction mixture was kept at 0 °C using an ice bath. An aqueous solution (1 mL) of $NaNO_2$ (0.63 g, 9.2 mmol) was added dropwise to generate the azonium intermediate, and the reaction mixture was stirred for 10 min. A solution of *m*-phenylenediamine (1.00 g, 9.27 mmol) and sodium hydroxide (1.00 g) in MeOH−H_2O (2:1, v/v; 15 mL) was kept at 0 °C. With stirring, the azonium intermediate was added dropwise to the *m*-phenylenediamine solution while maintaining the temperature of the reaction at 3−5 °C. After stirring for 30 min, water (200 mL) was added to induce precipitation of a red solid, which was isolated by filtration and washed thoroughly with water to furnish **8** (2.26 g, 7.17 mmol, yield = 93%). ^{1}H NMR (400 MHz, DMSO-d_6, 298 K): δ 7.56 (d, J = 9.0 Hz, 2H), 7.30 (d, J = 8.6 Hz, 1H), 6.74 (d, J = 9.0 Hz, 2H), 6.60 (s, 2H), 5.85−5.92 (dd, J = 8.6, 2.0 Hz, 1H), 5.86 (d, J = 2.0 Hz, 1H), 5.67 (s, 2H), 4.79 (t, J = 5.4 Hz, 2H), 3.58 (m, 4H), 3.48 (m, 4H); ^{13}C NMR (100 MHz, DMSO-d_6, 298 K): δ 151.5, 148.1, 146.1, 143.1, 129.2, 122.6, 111.2, 104.7, 97.6, 58.2, 53.3. FT-IR (thin film on NaCl, cm^{-1}): 3457, 3351, 3232, 2952, 2873, 1596, 1510, 1394, 1355, 1332, 1249, 1199, 1153, 1054, 1003, 892, 823. HRMS (ESI) calcd for $C_{16}H_{22}N_5O_2$ [M + H]$^+$ 316.1774; found 316.1780.

2-[(*N*,*N*-Bis(2-hydroxyethyl)-4-amino)phenyl]-2*H*-benzotriazol-5-amine (14). A stirred MeCN solution (10 mL) of **8** (125 mg, 0.397 mmol) and $Cu(OAc)_2{\cdot}H_2O$ (416 mg, 2.09 mmol) was heated at 80 °C for 30 min. Volatile fractions were removed under reduced pressure. The residual material was treated with an aqueous solution of EDTA (0.1 M, 50 mL) and extracted into EtOAc (5 × 100 mL). The combined extracts were dried over anhydrous $MgSO_4$, filtered, and concentrated. Flash column chromatography on SiO_2 (CH_2Cl_2:methanol = 10:1, v/v) furnished **14** as a bright-yellow solid (114 mg, 0.364 mmol, yield = 92%). ^{1}H NMR (400 MHz, DMSO-d_6, 298 K): δ 7.95 (d, J = 9.3 Hz, 2H), 7.63 (d, J = 9.0 Hz, 1H), 6.89−6.92 (dd, J = 9.0, 2.0 Hz, 1H), 6.82 (d, J = 9.0 Hz, 2H), 6.69 (d, J = 1.1 Hz, 1H), 5.48 (br s, 2H), 4.79 (br t, J = 5.5 Hz, 2H), 3.56−3.61 (q, J = 5.9 Hz, 4H), 3.47−3.50 (t, J = 5.8 Hz, 4H); ^{13}C NMR (100 MHz, DMSO-d_6, 298 K): δ 148.4, 148.1, 146.5, 139.3, 129.4, 121.6, 121.0, 118.2, 111.8, 93.3, 58.5, 53.7. FT-IR (thin film on NaCl, cm^{-1}): 3338, 3227, 2930, 2871, 1631, 1607, 1560, 1517, 1457, 1417, 1356, 1300, 1218, 1049, 1004, 816. HRMS (ESI) calcd for $C_{16}H_{20}N_5O_2$ [M + H]$^+$ 314.1617; found 314.1609.

■ ASSOCIATED CONTENT

Ⓢ Supporting Information

Synthesis and characterization of **4**−**7** and **10**−**13**; additional spectroscopic, kinetic, and X-ray crystallographic data. This material is available free of charge via the Internet at http://pubs.acs.org.

■ AUTHOR INFORMATION

Corresponding Author

dongwhan@indiana.edu

Notes

The authors declare no competing financial interest.

■ ACKNOWLEDGMENTS

This work was supported by DTRA/ARO (W911NF-07-1-0533).

■ REFERENCES

(1) (a) Czarnik, A. W. *Acc. Chem. Res.* **1994**, *27*, 302−308. (b) Fabbrizzi, L.; Poggi, A. *Chem. Soc. Rev.* **1995**, *24*, 197−202. (c) *Chemosensors of Ion and Molecule Recognition*; Desvergne, J. P.; Czarnik, A. W., Eds.; Kluwer Academic Publishers: Dordrecht, The Netherlands, 1997. (d) de Silva, A. P.; Gunaratne, H. Q. N.; Gunnlaugsson, T.; Huxley, A. J. M.; McCoy, C. P.; Rademacher, J. T.; Rice, T. E. *Chem. Rev.* **1997**, *97*, 1515−1566. (e) Amendola, V.; Fabbrizzi, L.; Licchelli, M.; Mangano, C.; Pallavicini, P.; Parodi, L.; Poggi, A. *Coord. Chem. Rev.* **1999**, *190*−*192*, 649−669. (f) McQuade, D. T.; Pullen, A. E.; Swager, T. M. *Chem. Rev.* **2000**, *100*, 2537−2574. (g) Valeur, B.; Leray, I. *Coord. Chem. Rev.* **2000**, *205*, 3−40. (h) de Silva, A. P.; Fox, D. B.; Huxley, A. J. M.; Moody, T. S. *Coord. Chem. Rev.* **2000**, *205*, 41−57. (i) Prodi, L.; Bolletta, F.; Montalti, M.; Zaccheroni, N. *Coord. Chem. Rev.* **2000**, *205*, 59−83. (j) Rurack, K.; Resch-Genger, U. *Chem. Soc. Rev.* **2002**, *31*, 116−127. (k) de Silva, A. P.; McCaughan, B.; McKinney, B. O. F.; Querol, M. *Dalton Trans.* **2003**, 1902−1913. (l) Martínez-Mánez, R.; Sancenón, F. *Chem. Rev.* **2003**, *103*, 4419−4476. (m) *Advanced Concepts in Fluorescence Sensing. Part A: Small Molecule Sensing*; Geddes, C. D.; Lakowicz, J. R., Eds.; Springer: New York, 2005; Vol. 9. (n) Thomas, S. W., III; Joly, G. D.; Swager, T. M. *Chem. Rev.* **2007**, *107*, 1339−1386. (o) Anslyn, E. V. *J. Org. Chem.* **2007**, *72*, 687−699. (p) Nolan, E. M.; Lippard, S. J. *Chem. Rev.* **2008**, *108*, 3443−3480. (q) Domaille, D. W.; Que, E. L.; Chang, C. J. *Nat. Chem. Biol.* **2008**, *4*, 168−175. (r) Nolan, E. M.; Lippard, S. J. *Acc. Chem. Res.* **2009**, *42*, 193−203. (s) Xu, Z.; Yoon, J.; Spring, D. R. *Chem. Soc. Rev.* **2010**, *39*, 1996−2006. (t) Lee, D. In *Chemosensors: Principles, Strategies, and Applications*; Wang, B., Anslyn, E. V., Eds.; John Wiley & Sons: Hoboken, NJ, 2011, p 41−64.

(2) (a) Que, E. L.; Domaille, D. W.; Chang, C. J. *Chem. Rev.* **2008**, *108*, 1517−1549. (b) Kim, B.-E.; Nevitt, T.; Thiele, D. J. *Nat. Chem. Biol.* **2008**, *4*, 176−185. (c) Boal, A. K.; Rosenzweig, A. C. *Chem. Rev.* **2009**, *109*, 4760−4779.

(3) (a) Bush, A. I. *Curr. Opin. Chem. Biol.* **2000**, *4*, 184−191. (b) Millhauser, G. L. *Acc. Chem. Res.* **2004**, *37*, 79−85. (c) Donnelly, P. S.; Xiao, Z.; Wedd, A. G. *Curr. Opin. Chem. Biol.* **2007**, *11*, 128−133. (d) Madsen, E.; Gitlin, J. D. *Annu. Rev. Neurosci.* **2007**, *30*, 317−337. (e) Gaggelli, E.; Kozlowski, H.; Valensin, D.; Valensin, G. *Chem. Rev.*

2006, *106*, 1995−2044. (f) Gh Popescu, B. F.; Nichol, H. *CNS Neurosci. Ther.* **2011**, *17*, 256−268.
(4) Bergonzi, R.; Fabbrizzi, L.; Licchelli, M.; Mangano, C. *Coord. Chem. Rev.* **1998**, *170*, 31−46.
(5) (a) Royzen, M.; Dai, Z.; Canary, J. W. J. *Am. Chem. Soc.* **2005**, *127*, 1612−1613. (b) Xu, Z.; Qian, X.; Cui, J. *Org. Lett.* **2005**, *7*, 3029−3032. (c) Xu, Z.; Xiao, Y.; Qian, X.; Cui, J.; Cui, D. *Org. Lett.* **2005**, *7*, 889−892. (d) Wen, Z.-C.; Yang, R.; He, H.; Jiang, Y.-B. *Chem. Commun.* **2006**, 106−108. (e) Goswami, S.; Sen, D.; Das, N. K. *Org. Lett.* **2010**, *12*, 856−859. (f) Xu, Z.; Pan, J.; Spring, D. R.; Cui, J.; Yoon, J. *Tetrahedron* **2010**, *66*, 1678−1683.
(6) For a phosphorescence-based copper(II) imaging agent, see: You, Y.; Han, Y.; Lee, Y.-M.; Park, S. Y.; Nam, W.; Lippard, S. J. *J. Am. Chem. Soc.* **2011**, *133*, 11488−11491.
(7) For recent review articles on reactivity-based chemical detection: (a) Yang, Y.; Zhao, Q.; Feng, W.; Li, F. *Chem. Rev.* 2012, *112*, ASAP. (b) Kaur, K.; Saini, R.; Kumar, A.; Luxami, V.; Kaur, N.; Singh, P.; Kumar, S. *Coord. Chem. Rev.* **2012**, *256*, 1992−2028. (c) Chen, X.; Pradhan, T.; Wang, F.; Kim, J. S.; Yoon, J. *Chem. Rev.* **2011**, *112*, 1910−1956. (d) Quang, D. T.; Kim, J. S. *Chem. Rev.* **2010**, *110*, 6280−6301. (e) Cho, D.-G.; Sessler, J. L. *Chem. Soc. Rev.* **2009**, *38*, 1647−1662.
(8) (a) Dujols, V.; Ford, F.; Czarnik, A. W. *J. Am. Chem. Soc.* **1997**, *119*, 7386−7387. (b) Kovács, J.; Rödler, T.; Mokhir, A. *Angew. Chem. Intl. Ed.* **2006**, *45*, 7815−7817. (c) Xiang, Y.; Tong, A.; Jin, P.; Ju, Y. *Org. Lett.* **2006**, *8*, 2863−2866. (d) Qi, X.; Jun, E. J.; Xu, L.; Kim, S.-J.; Hong, J. S. J.; Yoon, Y. J.; Yoon, J. *J. Org. Chem.* **2006**, *71*, 2881−2884. (e) Zhang, X.; Shiraishi, Y.; Hirai, T. *Org. Lett.* **2007**, *9*, 5039−5042. (f) Swamy, K. M. K.; Ko, S.-K.; Kwon, S. K.; Lee, H. N.; Mao, C.; Kim, J.-M.; Lee, K.-H.; Kim, J.; Shin, I.; Yoon, J. *Chem. Commun.* **2008**, 5915−5917. (g) Kim, M. H.; Jang, H. H.; Yi, S.; Chang, S.-K.; Han, M. S. *Chem. Commun.* **2009**, 4838−4840. (h) Zhao, Y.; Zhang, X.-B.; Han, Z.-X.; Qiao, L.; Li, C.-Y.; Jian, L.-X.; Shen, G.-L.; Yu, R.-Q. *Anal. Chem.* **2009**, *81*, 7022−7030. (i) Zhou, Y.; Wang, F.; Kim, Y.; Kim, S.-J.; Yoon, J. *Org. Lett.* **2009**, *11*, 4442−4445. (j) Yu, F.; Zhang, W.; Li, P.; Xing, Y.; Tong, L.; Ma, J.; Tang, B. *Analyst* **2009**, *134*, 1826−1833. (k) Wang, Q.-L.; Zhang, H.; Jiang, Y.-B. *Tetrahedron Lett.* **2009**, *50*, 29−31. (l) Li, N.; Xiang, Y.; Tong, A. *Chem. Commun.* **2010**, *46*, 3363−3365. (m) Zhang, J. F.; Zhou, Y.; Yoon, J.; Kim, Y.; Kim, S. J.; Kim, J. S. *Org. Lett.* **2010**, *12*, 3852−3855. (n) Kumar, M.; Kumar, N.; Bhalla, V.; Sharma, P. R.; Kaur, T. *Org. Lett.* **2012**, *14*, 406−409. (o) Zhao, C.; Feng, P.; Cao, J.; Wang, X.; Yang, Y.; Zhang, Y.; Zhang, J.; Zhang, Y. *Org. Biomol. Chem.* **2012**, *10*, 3104−3109. (p) Liu, W.-Y.; Li, H.-Y.; Zhao, B.-X.; Miao, J.-Y. *Analyst* **2012**, *137*, 3466−3469.
(9) (a) Liu, J.; Lu, Y. *J. Am. Chem. Soc.* **2007**, *129*, 9838−9839. (b) Liu, M.; Zhao, H.; Chen, S.; Yu, H.; Zhang, Y.; Quan, X. *Chem. Commun.* **2011**, *47*, 7749−7751.
(10) (a) Schmidt, M. P.; Hagenböcker, A. *Chem. Ber.* **1921**, *54*, 2191−2200. (b) Schmidt, M. P.; Hagenböcker, A. *Chem. Ber.* **1921**, *54*, 2201−2207.
(11) Nigh, W. G. In *Oxidation in Organic Chemistry*; Trahanovsky, W. S., Ed.; Academic Press: London, 1973; Vol. *5B*, pp 1−96.
(12) Carboni, R. A.; Kauer, J. C.; Castle, J. E.; Simmons, H. E. *J. Am. Chem. Soc.* **1967**, *89*, 2618−2625.
(13) Hall, J. H. *J. Org. Chem.* **1968**, *33*, 2954−2956.
(14) (a) Carboni, R. A.; Castle, J. E. *J. Am. Chem. Soc.* **1962**, *84*, 2453−2454. (b) Carboni, R. A.; Kauer, J. C.; Hatchard, W. R.; Harder, R. J. *J. Am. Chem. Soc.* **1967**, *89*, 2626−2633. (c) Kauer, J. C.; Carboni, R. A. *J. Am. Chem. Soc.* **1967**, *89*, 2633−2637.
(15) (a) Zincke, T.; Th Lawson, A. *Chem. Ber.* **1887**, *20*, 1176−1183. (b) Zincke, T.; Jaenke, H. *Chem. Ber.* **1888**, *21*, 540−548.
(16) Dyall, L. K. *Aust. J. Chem.* **1979**, *32*, 643−651.
(17) Griller, D.; Barclay, L. R. C.; Ingold, K. U. *J. Am. Chem. Soc.* **1975**, *97*, 6151−6154.
(18) Butler, R. N. *Chem. Rev.* **1984**, *84*, 249−276.
(19) (a) Turro, N. J. *Modern Molecular Photochemistry*; University Science Books: Sausalito, CA, 1991. (b) Lakowicz, J. R. *Principles of Fluorescence Spectroscopy*; 3rd ed.; Springer: New York, 2006. (c) Valeur, B. *Molecular Fluorescence: Principles and Applications*; Wiley-VCH: Weinheim, Germany, 2002.
(20) (a) Reichardt, C. *Chem. Rev.* **1994**, *94*, 2319−2358. (b) Reichardt, C.; Welton, T. *Solvents and Solvent Effects in Organic Chemistry*; 4th ed.; Wiley-VCH: Weinheim, 2010.
(21) Externally referenced to the Fc/Fc^+ redox couple.
(22) (a) Burlov, A. S.; Uraev, A. I.; Lysenko, K. A.; Chigarenko, G. G.; Ponomarenko, A. G.; Matuev, P. V.; Nikolaevskii, S. A.; Garnovskaya, E. D.; Borodkin, G. S.; Garnovskii, A. D. *Russ. J. Coord. Chem.* **2006**, *32*, 686−691. (b) Burlov, A. S.; Uraev, A. I.; Matuev, P. V.; Lysenko, K. A.; Kamkin, N. N.; Garnovskii, D. A.; Nikolaevskii, S. A.; Kogan, V. A.; Garnovskii, A. D. *Russ. J. Coord. Chem.* **2008**, *34*, 904−910. (c) Price, R.; Yates, J. E. *J. Chem. Soc., Perkin Trans. 1* **1982**, 1775−1782. (d) Liss, T. A.; Baer, D. R. *Inorg. Chem.* **1969**, *8*, 1328−1336.
(23) For structurally characterized azoaminoaromatics having similar N−H···N bond as part of a six-membered ring structure, see: (a) Maciejewska, D.; Wolska, I.; Kowalska, V. *J. Mol. Str.* **2004**, *693*, 27−34. (b) Kelemen, J.; Kormány, G.; Rihs, G. *Dyes Pigm.* **1982**, *3*, 249−271.
(24) See Scheme 5 for the designation of the Nα and Nβ atoms of the azo group.
(25) For structurally characterized azoaminoaromatics having similar N−H···N bond as part of a five-membered ring structure, see: (a) Zhang, L.; Xia, J.; Li, Q.; Li, X.; Wang, S. *Organometallics* **2011**, *30*, 375−378. (b) Bohle, D. S.; Dorans, K. S.; Fotie, J. *Acta Crystallogr.* **2007**, *E63*, o889−o890.
(26) *The Chemistry of the hydrazo, azo and azoxy groups*; Patai, S., Ed.; John Wiley & Sons: London, 1975.
(27) Sawicki, E. *J. Org. Chem.* **1957**, *22*, 915−919.
(28) Considering the rotameric relationship between **7A′** and **7B′** with minor structural variation, contributions of solvation and entropic factors to the overall Gibbs free energy would essentially cancel out. Therefore, the purely electronic energy difference should be a good approximation of the intrinsic thermodynamic preference even in the solution state.
(29) The lack of reactivity (pH < 5.5) presumably reflects the difficulty in the mechanistically required (Scheme 3) deprotonation steps in acidic environment.
(30) The fluorescence response of **8** toward copper(II) becomes less pronounced in the presence of a large excess of iron(II) in solution (Figure 8d). As shown in Figure S8, ca. 50% decrease in the fluorescence intensity at λ = 530 nm was indeed observed upon treating the cyclization product **14** with 100 equiv of iron(II) in buffered (pH = 7.0; HEPES, 50 mM) water. This finding suggests that the presence of iron(II) does not interfere with the oxidative cyclization of **8**, which is effected exclusively by copper(II) among all the metal ions screened in Figure 8d. The decrease in the emission intensity rather reflects partial quenching of the fluorescence of the reaction product **14**, presumably through interaction with paramagnetic iron(II) species in solution.
(31) *Edition of the Drinking Water Standards and Health Advisories (EPA 822-S-12−001)*; U.S. EPA Office of Science and Technology: Washington, D.C., 2012.
(32) Ferlin, M. G.; Via, L. D.; Gia, O. M. *Bioorg. Med. Chem.* **2004**, *12*, 771−777.
(33) Bléger, D.; Ciesielski, A.; Samorí, P.; Hecht, S. *Chem.—Eur. J.* **2010**, *16*, 14256−14260.
(34) Williams, A. T. R.; Winfield, S. A.; Miller, J. N. *Analyst* **1983**, *108*, 1067−1071.